AIAA JOURNAL
Vol. 42, No. 5, May 2004

Analytical Euler Solution for Two-Dimensional Compressible Ramp Flow with Experimental Comparison

A. Verhoff*
Florissant, Missouri 63031

A newly developed procedure for obtaining analytical asymptotic solutions of the two-dimensional steady-state Euler equations is applied to compressible flow past a ramp to further demonstrate its general utility. The procedure has been shown to be applicable into the low transonic range (shock free). The equations are written in natural streamline coordinates with mass flux and flow angle as dependent variables. Higher-order effects, for example, compressibility, appear as nonhomogeneous forcing terms. This new solution procedure does not require a Green's function for the forcing terms and has general applicability to many other disciplines, for example, heat transfer, besides fluid dynamics. Application of the new approach to flow problems having geometric corners, for example, ramp, reveals the typical singularity compounding at higher order. The analytical nature of the solution guides implementation of a nonconformal mapping and a new type of coordinate straining strategy to control the phenomenon and ensure uniform validity. Understanding of the nature of the inviscid flow near a geometric corner can be used to devise improved computational fluid dynamics surface boundary conditions at such singular points, for example, airfoil trailing edge. The analytical validity of the ramp solution is corroborated for this purpose by the von Kármán similarity rule; its predictions also compare favorably with test data.

Nomenclature

a	=	speed of sound (nondimensionalized by stagnation speed of sound)
b, d	=	solution-plane mapping parameter
D_0	=	simplifying factor, $\sqrt{(\tau\bar{\tau})}$
D_1	=	simplifying factor, $\sqrt{[(\tau-1)(\bar{\tau}-1)]}$
F	=	complex dependent variable, $T - i\theta$
$\bar{F}$	=	complex conjugate of dependent variable F
G	=	mapping function
$\bar{G}$	=	complex conjugate of mapping function G
H	=	analytic homogeneous solution
h_1, h_2	=	corner point functions of Δ
i	=	complex number, $\sqrt{-1}$
k	=	asymptotic expansion index
M	=	local Mach number
M_∞	=	freestream Mach number
M_∞^*	=	critical freestream Mach number
n, s	=	streamline-plane coordinate
$\bar{n}$	=	coordinate aligned with streamline-normal direction
p	=	local pressure (nondimensionalized by stagnation pressure)
p_c	=	pressure at corner point nondimensionalized by stagnation pressure
p_∞	=	freestream pressure nondimensionalized by stagnation pressure
Q	=	logarithm of local velocity nondimensionalized by freestream velocity
q	=	local velocity (nondimensionalized by stagnation speed of sound)
q_c	=	velocity at corner point nondimensionalized by stagnation speed of sound
q_k	=	asymptotic expansion component of $\bar{q}$, where $k = 1, 2, 3, \ldots$
$\bar{q}_0$	=	zero-order velocity nondimensionalized by freestream velocity
q_∞	=	freestream velocity nondimensionalized by stagnation speed of sound
$\bar{q}$	=	local velocity nondimensionalized by freestream velocity
$(q)_E$	=	expansion corner velocity nondimensionalized by stagnation speed of sound
$(\bar{q})_E$	=	expansion corner velocity nondimensionalized by freestream velocity
R	=	radius of arc in solution plane
r	=	radius of arc in solution plane
$r_k, F_k, G_k, H_k, R_k, T_k, \theta_k$	=	asymptotic expansion component of r, F, G, H, R, T, and θ, where $k = 0, 1, 2, 3, \ldots$
S	=	entropy
$\bar{s}$	=	coordinate aligned with streamline direction
T	=	logarithm of mass flux nondimensionalized by freestream mass flux
t	=	body thickness ratio
U, V	=	right-hand-side function of q
$(U-V)_\infty$	=	far-field value of $U - V$
u, v	=	solution-plane coordinate
w	=	solution-plane complex variable, $u + iv$
x, y	=	physical-plane coordinate
z	=	physical-plane complex variable, $x + iy$
$\bar{z}$	=	complex conjugate of z, $x - iy$
α	=	ramp angle
Γ	=	von Kármán scaling parameter
γ	=	ratio of specific heats
Δ	=	corner turning angle
δ, ν	=	coordinate straining parameter
ε	=	expansion parameter
$\hat{\varepsilon}$	=	similarity variable
ε^*	=	critical value of ε
ζ	=	coordinate-straining-plane complex variable, $\xi + i\eta$
$\bar{\zeta}$	=	complex conjugate of ζ, $\xi - i\eta$
ξ, η	=	coordinate-straining-plane coordinate
θ	=	local flow angle
λ	=	von Kármán similarity parameter
ρ	=	local density nondimensionalized by stagnation density
ρ_c	=	density at corner point nondimensionalized by stagnation density

Received 13 August 2002; revision received 21 June 2003; accepted for publication 2 September 2003. Copyright © 2004 by the American Institute of Aeronautics and Astronautics, Inc. All rights reserved. Copies of this paper may be made for personal or internal use, on condition that the copier pay the $10.00 per-copy fee to the Copyright Clearance Center, Inc., 222 Rosewood Drive, Danvers, MA 01923; include the code 0001-1452/04 $10.00 in correspondence with the CCC.

*Retired, 108 Rosebrook Drive. Associate Fellow AIAA.

ρ_∞	=	freestream density nondimensionalized by stagnation density
σ	=	surface arc length
τ	=	streamline-plane complex variable, $s + in$
$\bar{\tau}$	=	complex conjugate of τ, $s - in$
Φ	=	additive straining function
ϕ_k	=	asymptotic expansion component, where $k = 1, 2, 3, \ldots$
ψ, ω	=	coordinate-straining-plane polar angle

Introduction

A NEW approach was introduced in Ref. 1 for obtaining analytical asymptotic solutions of the two-dimensional steady-state Euler equations. The equations are written uniquely in terms of mass flux and flow angle such that higher-order compressibility and rotationality effects appear as right-hand-side (RHS) forcing terms. A complex-variable mapping is then applied to this nonhomogeneous Cauchy–Riemann system resulting in a single first-order partial differential equation (PDE) in the complex plane.

This single PDE is solved by asymptotic iterative correction whereby the RHS terms are evaluated using previous iteration results. The new procedure allows closed-form analytical solutions to the resulting PDE at each order of approximation, provided the RHS terms are analytically defined. In this case the solution procedure is reduced to the evaluation of indefinite integrals. The procedure is general and applicable to the two-dimensional Poisson equation and its various subsets, such as nonhomogeneous Cauchy–Riemann systems, and the two-dimensional nonhomogeneous biharmonic equation. Therefore, it has applicability to many other disciplines, such as heat transfer, structures, etc.

The choice of mass flux and flow angle as dependent variables leads to a stronger set of boundary conditions for a given problem. At a solid surface the usual condition of tangential flow, that is, zero normal velocity, does not fix the velocity direction, which leads to the necessity of a Kutta condition to remove the ambiguity. Tangential flow with a prescribed direction can be imposed when flow angle is used. Mass flux as a dependent variable offers the advantage of being bounded, which is a property that can be exploited in assessing the validity and accuracy of a given solution. With the new mass flux formulation, the procedure is extendable to transonic shock-free flow (Ref. 2) because each value of mass flux corresponds to both a subsonic and a supersonic value of velocity.

The new Euler formulation and solution procedure are applied herein to compressible flow past a ramp of arbitrary inclination angle, that is, thickness ratio. This configuration provides a convenient (and simple) geometry for illustrating the nature of the solution singularity near the corners at higher order. Compounding of the singularity at higher order is suppressed by appealing to a nonconformal complex-variable coordinate straining. A new strategy is then introduced to ensure uniform validity. This approach can provide a detailed description of flow characteristics near geometric corners and resolve inconsistencies arising from employing classical potential flow solutions as models for local flow behavior. Such solutions can also provide the basis for devising improved computational fluid dynamics (CFD) surface boundary conditions at geometric singularities.

As an example of inconsistency arising from a potential flow model, the incompressible potential flow past a two-dimensional infinite wedge obtained by conformal mapping has been proposed for describing flow near a sharp leading or trailing edge. With this model, the flow stagnates at the apex. The presumption that velocity is small near a compression corner is used to justify incompressible wedge flow as a model even when compressibility effects are significant elsewhere in the flowfield. The major deficiency of this model is the absence of a uniform freestream velocity because the velocity increases without limit at large distances from the corner. This is discussed in more detail in Ref. 3.

Relying on the incompressible flow solution to infer behavior near a geometric corner leads to major inconsistencies between cause and effect. For example, the incompressible solution for the ramp geometry in Fig. 1 can be obtained by conformal mapping. This solution has the flow stagnating at the compression corner and velocity becoming infinite at the expansion corner for all ramp angles. A very low freestream velocity and a very small inclination angle, that is, small perturbations, produce an unbounded effect at the expansion corner, which is clearly inconsistent. Conventional arguments to dismiss the inconsistency state that compressibility would produce a shock wave, or that a real viscous flow would separate. These arguments are not very plausible for low freestream velocity. On the other hand, for subsonic freestream Mach numbers near 1, a very small ramp angle, that is, a small perturbation, produces a finite effect, that is, stagnation, at the compression corner, which is also inconsistent. In either case, the incompressible model is clearly deficient, which indicates that the neglected compressibility terms play an important role in the neighborhood of geometric singularities. (Note the absence of such inconsistencies for supersonic conditions.) Furthermore, the notion that compressible inviscid flow stagnates at an airfoil trailing edge leads to difficulties at transonic conditions when upper and lower surface streamlines having different entropy, that is, different total pressure resulting from a shock wave, merge at the trailing edge.

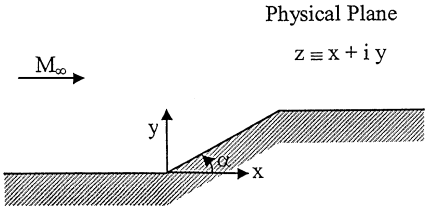

Fig. 1 Ramp geometry.

These issues of consistency were addressed in Refs. 3 and 4. In Ref. 4 a coordinate straining was used to suppress singular behavior at a geometric corner. However, extension of the approach to higher order was not straightforward. The extension presented there can also be shown to be mildly divergent. The present analysis rectifies these shortcomings.

Analytical solutions for the ramp geometry of Fig. 1 that illustrate the effects of compressibility on the nature of the flow near a corner are presented. The validity of these solutions is corroborated by the von Kármán similarity rule (see Ref. 5) near transonic conditions. This first-order rule is applicable at all Mach numbers under the restriction of small perturbations from freestream conditions. Predictions of critical freestream Mach number, that is, when the expansion corner velocity becomes sonic, are compared with limited test data. Surface Mach number predictions are also compared with experimental data.

Mass Flux Formulation

The analytical formulation in terms of mass flux and flow angle is presented in this section, including the mapping to streamline coordinates. The Euler equations are reduced to a nonhomogeneous Cauchy–Riemann system.

For two-dimensional steady flows the Euler equations can be written in streamline-oriented coordinates $\bar{s}$ and $\bar{n}$ as

$$\frac{\partial\theta}{\partial\bar{s}} - \frac{\partial Q}{\partial\bar{n}} = \frac{1}{M^2}\frac{\partial S}{\partial\bar{n}}, \qquad \frac{\partial\theta}{\partial\bar{n}} + (1 - M^2)\frac{\partial Q}{\partial\bar{s}} = 0$$

$$a^2 + \frac{\gamma - 1}{2}q^2 = 1 \tag{1}$$

Velocity magnitude and speed of sound (both nondimensionalized by stagnation speed of sound) are denoted by q and a, respectively, and Q is the logarithm of velocity q normalized by the freestream value q_∞ (also nondimensionalized by stagnation speed of sound). The local Mach number is M and entropy S is defined in terms of pressure p and density ρ as

$$S \equiv [1/\gamma(\gamma - 1)]\,\ell_n(p/\rho^\gamma) = S(\bar{n}) \tag{2}$$

It is evident from the algebraic energy equation (1) that pressure and density are nondimensionalized by their respective stagnation values. The flow angle is θ and local distances along and normal to the streamline direction are denoted by $\bar{s}$ and $\bar{n}$, respectively. Density

can be expressed as a function of velocity magnitude and entropy according to

$$\rho = \{1 - [(\gamma - 1)/2]q^2\}^{1/(\gamma-1)} e^{-\gamma S} \tag{3}$$

The formulation for isentropic flow will be used for the ramp flow application.

Streamlines and their normals are defined by the mapping

$$\frac{\partial s}{\partial x} = q\cos\theta, \qquad \frac{\partial s}{\partial y} = q\sin\theta$$
$$\frac{\partial n}{\partial x} = -\rho q\sin\theta, \qquad \frac{\partial n}{\partial y} = \rho q\cos\theta \tag{4}$$

A correction would be required for nonisentropic conditions. The coordinates s and n represent velocity potential and stream function, respectively. The relationships

$$\frac{\partial s}{\partial \bar{s}} = q, \qquad \frac{\partial s}{\partial \bar{n}} = 0, \qquad \frac{\partial n}{\partial \bar{s}} = 0, \qquad \frac{\partial n}{\partial \bar{n}} = \rho q \tag{5}$$

transform the isentropic Euler equations to streamline coordinates as

$$\frac{\partial \theta}{\partial s} - \frac{\partial Q}{\partial n} = (\rho - 1)\frac{\partial Q}{\partial n}, \qquad \frac{\partial \theta}{\partial n} + \frac{\partial Q}{\partial s} = \left(1 - \frac{1}{\rho} + \frac{M^2}{\rho}\right)\frac{\partial Q}{\partial s} \tag{6}$$

When relation (3) is used, the density can be represented (for isentropic conditions) by its binomial expansion

$$\rho = 1 - (1/2)q^2 + (1/8)(2-\gamma)q^4 - (1/48)(2-\gamma)(3-2\gamma)q^6 + \cdots \tag{7}$$

which is uniformly convergent for all Mach numbers and is rapidly convergent well into the supersonic range. Note that entropy effects can be introduced as a multiplicative factor to this expression. By the definition of a new dependent variable T as

$$T \equiv \ell_n(\rho q/\rho_\infty q_\infty) \tag{8}$$

and the introduction of expansion (7), the isentropic Euler equations (6) become

$$\frac{\partial \theta}{\partial s} - \frac{\partial T}{\partial n} = \frac{\partial U}{\partial n}, \qquad \frac{\partial \theta}{\partial n} + \frac{\partial T}{\partial s} = \frac{\partial V}{\partial s} \tag{9}$$

The functions U and V have the asymptotic representations

$$U \equiv (1/4)q^2 + (1/32)(3\gamma - 2)q^4 + (1/288)(10\gamma^2 - 17\gamma + 6)q^6 + \cdots$$
$$V \equiv -(1/4)q^2 + (1/32)(4-\gamma)q^4 - (1/288)(2\gamma^2 - 19\gamma + 12)q^6 + \cdots \tag{10}$$

which depend only on the local velocity (or local Mach number).

The functions U and V are rapidly convergent well into the supersonic range without reliance on a small perturbation parameter. A formal expansion parameter ε (for tracking the order of terms in the analysis) can nevertheless be introduced defined as

$$\varepsilon \equiv \tfrac{1}{4}q_\infty^2 = \tfrac{1}{4}\left(M_\infty^2 \Big/ \left\{1 + [(\gamma-1)/2]M_\infty^2\right\}\right) \tag{11}$$

This dimensionless parameter is artificial and is not assumed to be necessarily small. It is bounded for all freestream Mach numbers; for small M_∞ it is proportional to the Janzen–Rayleigh perturbation parameter (see Ref. 6). It also serves to decouple freestream conditions from the solution process. When ε is introduced, the functions U and V then become

$$U = \varepsilon\bar{q}^2 + \tfrac{1}{2}\varepsilon^2(3\gamma-2)\bar{q}^4 + \tfrac{2}{9}\varepsilon^3(10\gamma^2 - 17\gamma + 6)\bar{q}^6 + \cdots$$
$$V = -\varepsilon\bar{q}^2 + \tfrac{1}{2}\varepsilon^2(4-\gamma)\bar{q}^4 - \tfrac{2}{9}\varepsilon^3(2\gamma^2 - 19\gamma + 12)\bar{q}^6 + \cdots \tag{12}$$

where the normalized velocity is defined as

$$\bar{q} \equiv q/q_\infty \tag{13}$$

Because the functions U and V have expansions in terms of the parameter ε, the dependent variables T and θ along with velocity q can likewise be expanded as

$$T = T_0 + \varepsilon T_1 + \varepsilon^2 T_2 + \varepsilon^3 T_3 + \cdots$$
$$\theta = \theta_0 + \varepsilon\theta_1 + \varepsilon^2\theta_2 + \varepsilon^3\theta_3 + \cdots$$
$$\bar{q} = \bar{q}_0\left[1 + \varepsilon q_1 + \varepsilon^2 q_2 + \varepsilon^3 q_3 + \cdots\right] \tag{14}$$

Making use of the density expansion (7) and the definition (8) leads to the relationships

$$\bar{q}_0 = e^{T_0}$$
$$q_1 = T_1 + 2\bar{q}_0^2 - 2$$
$$q_2 = T_2 - 2T_1 + \tfrac{1}{2}T_1^2 + 6q_1\bar{q}_0^2 - 2(2-\gamma)\left[\bar{q}_0^4 - 1\right]$$
$$\vdots \tag{15}$$

System (9) can be viewed as linear, nonhomogeneous partial differential equations assuming that the RHS terms U and V are known quantities. In an asymptotic corrective iteration process, these terms, if they are reasonably small and well behaved, can be approximated using previous iteration results, and their integration yields a more refined approximation. Solution of the homogeneous left-hand-side portion, which depends on mass flux and contains some compressibility effects, provides an initial starting approximation. On convergence, the process yields the shock-free solution of the Euler equations (9). This procedure is dissimilar to previous asymptotic analyses appearing in the literature, which typically employ a small perturbation parameter, for example, freestream Mach number, thickness ratio, etc., and use an incompressible solution as the zero-order term in the expansion. The range of validity of these classical approaches is typically limited by some radius of convergence.

Solution Procedure

The new solution process introduced in Ref. 1 for the nonhomogeneous equations is outlined in this section. Provided the RHS terms are analytically defined, closed-form analytical solutions can be obtained readily even when the RHS terms are functionally complicated. The procedure does not require a Green's function.

Introduction of the new complex dependent variable

$$F \equiv T - i\theta \tag{16}$$

and the complex-variable mapping

$$s = \tfrac{1}{2}(\bar{\tau} + \tau), \qquad n = (i/2)(\bar{\tau} - \tau)$$
$$\tau \equiv s + in, \qquad \bar{\tau} \equiv s - in \tag{17}$$

transforms the Euler system (9) into the single first-order PDE

$$\frac{\partial F}{\partial \bar{\tau}} = \frac{1}{2}\frac{\partial}{\partial \tau}(U + V) - \frac{1}{2}\frac{\partial}{\partial \bar{\tau}}(U - V) \tag{18}$$

The new dependent variable F has the expansion

$$F = F_0 + \varepsilon F_1 + \varepsilon^2 F_2 + \varepsilon^3 F_3 + \cdots \tag{19}$$

which follows from expansions (14).

If a conformal mapping represented by

$$\tau = G(\zeta), \qquad \zeta \equiv \xi + i\eta \tag{20}$$

is introduced, the Euler system becomes

$$\frac{\partial F}{\partial \bar{\zeta}} = \frac{1}{2}\left(\frac{\partial G}{\partial \zeta}\right)^{-1}\frac{\partial \bar{G}}{\partial \bar{\zeta}}\frac{\partial}{\partial \zeta}(U + V) - \frac{1}{2}\frac{\partial}{\partial \bar{\zeta}}(U - V) \tag{21}$$

Integration yields

$$F = \frac{1}{2}\left(\frac{\partial G}{\partial \zeta}\right)^{-1}\frac{\partial}{\partial \zeta}\int (U + V)\frac{\partial \bar{G}}{\partial \bar{\zeta}}\,\mathrm{d}\bar{\zeta} - \frac{1}{2}(U - V) + \frac{1}{2}(U - V)_\infty + H(\zeta) \tag{22}$$

where $(U-V)_\infty$ represents the far-field value. The homogenous solution $H(\zeta)$ provides the means for imposing corrections to maintain boundary condition fidelity necessitated by the indefinite integration.

If a nonconformal mapping represented by

$$\tau = G(\zeta, \bar{\zeta}), \qquad \bar{\zeta} \equiv \xi - i\eta \tag{23}$$

is introduced rather than mapping (20), the Euler system becomes

$$\frac{\partial F}{\partial \bar{\zeta}}\frac{\partial G}{\partial \zeta} = \frac{\partial F}{\partial \zeta}\frac{\partial G}{\partial \bar{\zeta}} + \frac{1}{2}\frac{\partial \bar{G}}{\partial \bar{\zeta}}\frac{\partial}{\partial \zeta}(U+V) - \frac{1}{2}\frac{\partial \bar{G}}{\partial \zeta}\frac{\partial}{\partial \bar{\zeta}}(U+V) + \frac{1}{2}\frac{\partial G}{\partial \bar{\zeta}}\frac{\partial}{\partial \zeta}(U-V) - \frac{1}{2}\frac{\partial G}{\partial \zeta}\frac{\partial}{\partial \bar{\zeta}}(U-V) \tag{24}$$

This expression is slightly more complicated than Eq. (21) for the case of a conformal mapping. For a coordinate-straining-type mapping, the function G has the expansion

$$\tau = \zeta + \varepsilon G_1(\zeta, \bar{\zeta}) + \varepsilon^2 G_2(\zeta, \bar{\zeta}) + \cdots \tag{25}$$

For the conformal mapping case the functions G_k depend on ζ only.

Convergence characteristics of the RHS quantities $U+V$ and $U-V$ appearing in the generating equations (18), (21), and (24) are shown in Figs. 2 and 3, respectively, as a function of local Mach number. Convergence is rapid into the supersonic range. Because the functions $U+V$ and $U-V$ are of higher order [see Eqs. (12)], Eq. (22) can be solved by corrective iteration. The zero-order solution F_0 corresponding to the homogeneous portion of system (9) provides the first approximation. At each level of asymptotic approximation during the solution process, an additional term in the series expansions (12) is included in the RHS forcing terms and the process is repeated to generate an improved approximation. With this process, the solution at each level of approximation is determined without altering previously determined lower-order components. There is no small expansion parameter per se (because ε is artificial) involved in the procedure; it relies on the rapid-convergence properties of expansions (10). This also holds true for the solution of Eqs. (18) and (24).

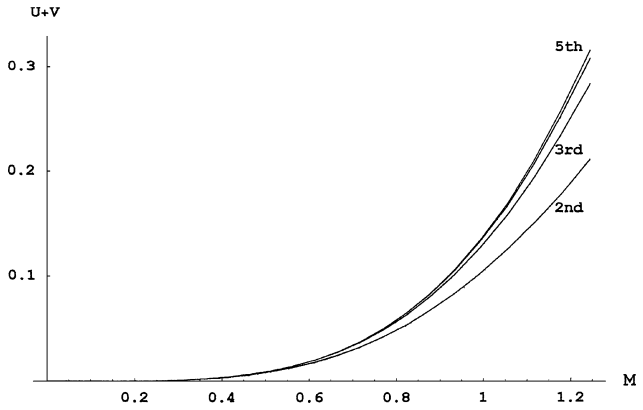

Fig. 2 Convergence characteristics of $U+V$ as a function of local Mach number.

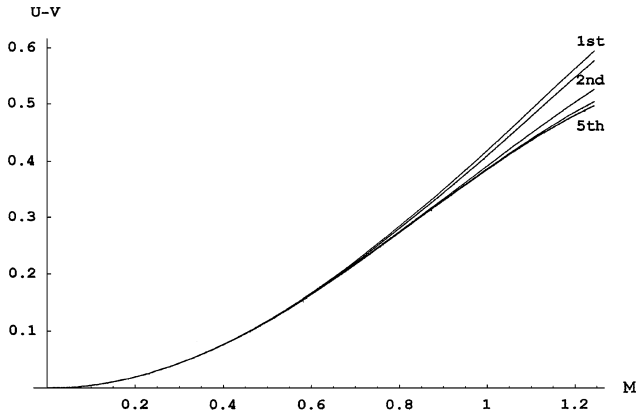

Fig. 3 Convergence characteristics of $U-V$ as a function of local Mach number.

Ramp Flow Application

Application of the preceding solution procedure to flow past a ramp of inclination angle α is presented in this section. The geometry is in Fig. 1. The ramp angle can be positive or negative and is not necessarily small. The projection of the physical plane onto the streamline plane, including the Dirichlet boundary conditions, is shown in Fig. 4. The compression corner maps to $\tau = 0$ and the expansion corner to $\tau = 1$.

Because the RHS of the generating equation (18) is of higher order, substitution of expansion (19) yields the zero-order equation

$$\frac{\partial F_0}{\partial \bar{\tau}} = 0 \tag{26}$$

This implies that F_0 is an analytic function of τ in the asymptotic sense. The first-order equation and its solution are

$$\frac{\partial F_1}{\partial \bar{\tau}} = -\frac{1}{2}\frac{\partial}{\partial \bar{\tau}}(U-V) \tag{27}$$

$$F_1 = -\left[\frac{1}{2}(U-V)_1 - \frac{1}{2}(U-V)_{1\infty}\right] + H_1(\tau) = 1 - e^{2T_0} \qquad (= T_1) \tag{28}$$

This last result is obtained from Eqs. (12), (14), and (15). Note that T_0 is the real part of F_0 and is generally a function of both τ and $\bar{\tau}$. The analytic function $H_1(\tau)$ provides for satisfying boundary conditions, but is not needed because F_1 is real. Higher-order solutions can be generated in a similar fashion.

Because the zero-order solution is indicated to be analytic, application of the Poisson integral formula to the upper half-plane Dirichlet problem of Fig. 4 provides the solution

$$\begin{aligned} F_0 &= (\alpha/\pi)\log[\tau/(\tau-1)], \qquad \tau \equiv s + in \\ T_0 &= (\alpha/2\pi)\,\ell_n\{(s^2+n^2)/[(s-1)^2+n^2]\} \\ \theta_0 &= (\alpha/\pi)\{\tan^{-1}[n/(s-1)] - \tan^{-1}(n/s)\} \end{aligned} \tag{29}$$

The real axis boundary conditions for this solution have $\theta = \alpha$ for $0 \le s \le 1$ and $\theta = 0$ elsewhere.

To zero order the normalized mass flux is

$$\rho q/\rho_\infty q_\infty = \{(s^2+n^2)/[(s-1)^2+n^2]\}^{\alpha/2\pi} \tag{30}$$

At the compression corner, $\tau = 0$, stagnation is predicted for all ramp angles, even for vanishingly small values of α. This leads to the unrealistic situation where an infinitesimal geometric perturbation produces a finite effect, that is, stagnation. For $\alpha = \pi/2$, stagnation is the correct condition. Thus, nonzero velocity must exist at smaller angles, with freestream conditions being approached at $\tau = 0$ as α vanishes. At the expansion corner, infinite mass flux is predicted

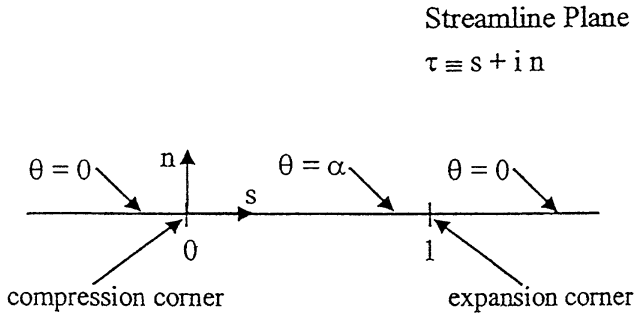

Fig. 4 Projection of physical plane onto streamline plane.

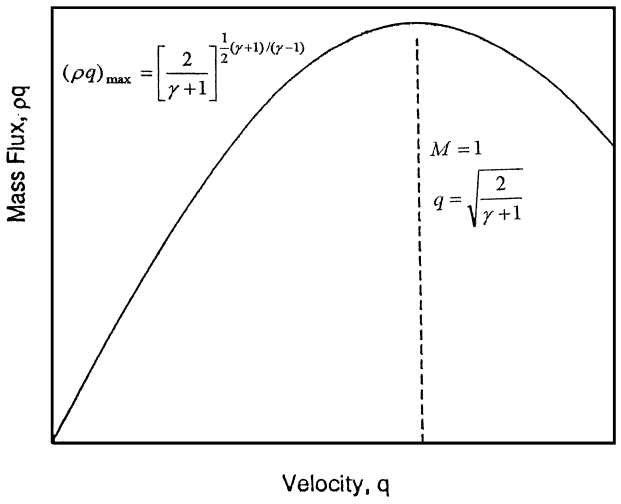

Fig. 5 Mass flux variation with velocity.

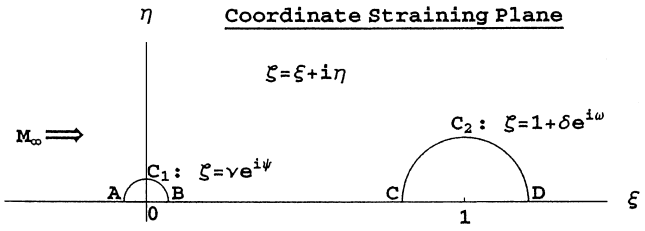

Fig. 6 Projection of streamline plane onto coordinate-straining plane.

by solution (30), even for vanishing α. This is physically incorrect because mass flux is bounded. (Mass flux as a function of velocity magnitude is shown in Fig. 5.) Furthermore, this singular-type behavior is compounded at higher order [see solution (28)], which is a clear indication of an incorrect formulation. The classical remedy for this situation is a coordinate straining.

Coordinate Straining

Straightforward solution of the generating equation (18) produces an asymptotic representation of the true solution in terms of the artificial parameter ε. The fact that the zero-order solution (29) is logarithmically singular at $\tau = 1$ implies that F_0 also has a local dependence on $\bar{\tau}$ (complex conjugate) in addition to τ. This dependence on $\bar{\tau}$ decays rapidly away from the singularity, leaving the dependence on τ indicated in solution (29). This local behavior is not captured properly by the straightforward approach so that a local coordinate straining must be introduced. A local straining is also called for at the compression corner to eliminate the physical inconsistencies at $\tau = 0$ discussed earlier.

Coordinate straining is arbitrary to a certain extent.[7] For the ramp problem, a suitable complex-variable straining is given by

$$\zeta = \frac{1}{2} + \frac{1}{2}(\tau - 1)\sqrt{1 + \frac{2\delta^2(\tau + \bar{\tau})}{(\tau - 1)(\bar{\tau} - 1)}} + \frac{\tau}{2}\sqrt{1 + \frac{2\nu^2(2 - \tau - \bar{\tau})}{\tau\,\bar{\tau}}} = G(\tau, \bar{\tau}) \tag{31}$$

This nonanalytic mapping from the streamline plane is shown schematically in Fig. 6. The arc C_1 maps to the single point $\tau = 0$, whereas the arc C_2 maps to $\tau = 1$. Along each of these semicircular arcs the dependent variable T takes on a constant value. This leads to a mixed boundary value (Dirichlet–Neumann) problem. These straining properties can be expressed as

$$\lim_{\tau \to 0}\{\zeta\} = \nu e^{i\psi}, \qquad \lim_{\tau \to 1}\{\zeta\} = 1 + \delta e^{i\omega}, \qquad \lim_{\tau \to \infty}\{\zeta - \tau\} = 0 \tag{32}$$

where $0 \le \psi \le \pi$ and $0 \le \omega \le \pi$. Presumably the parameters δ and ν are small.

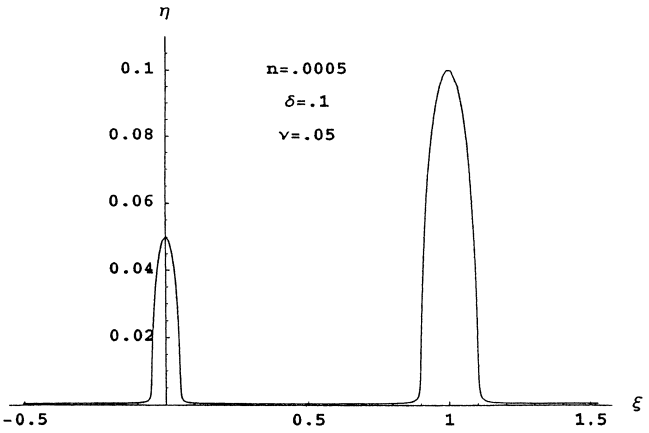

Fig. 7 Variation of η for streamline close to boundary, $n = 0.0005$, $\delta = 0.10$, and $\nu = 0.05$.

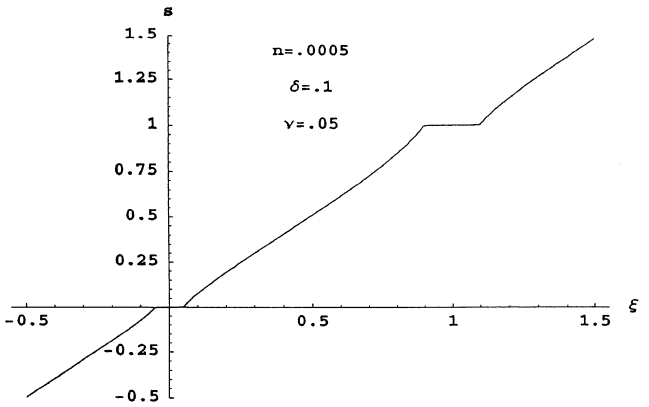

Fig. 8 Variation of s for streamline close to boundary, $n = 0.0005$, $\delta = 0.10$, and $\nu = 0.05$.

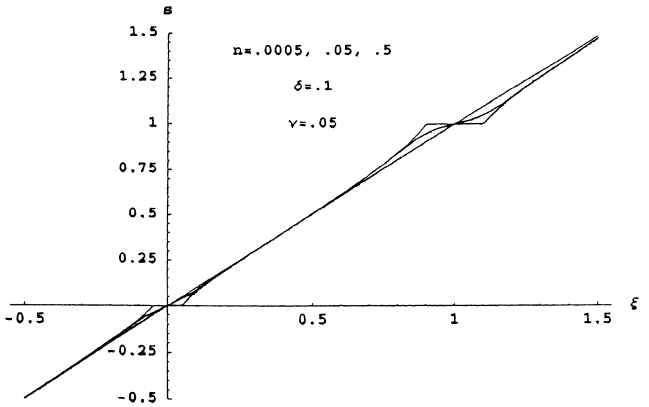

Fig. 9 Straining function characteristics near boundary.

The variation of the quantities η and s along a streamline close to the boundary (that is, $n = 0.0005$) is shown in Figs. 7 and 8, respectively, for arbitrarily chosen values of δ and ν. The local nature of the straining is evident in Fig. 9, which shows the variation of s for $n = 0.05$ and $n = 0.5$ in addition to that for $n = 0.0005$. Properties (32) along with the parameters δ and ν can be exploited to make the higher-order solutions physically consistent and uniformly valid.

Zero-Order Solution

The coordinate straining (31) transforms the generating equation (18) to the ζ plane. To zero order (in ε), the generating equation (24) becomes

$$\frac{\partial F_0}{\partial \bar{\zeta}}\frac{\partial G}{\partial \zeta} - \frac{\partial F_0}{\partial \zeta}\frac{\partial G}{\partial \bar{\zeta}} = 0 \tag{33}$$

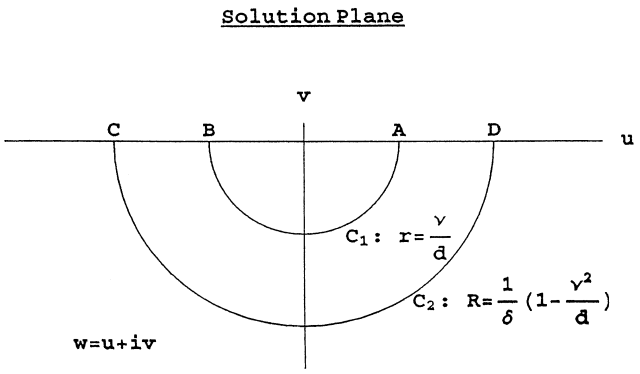

Fig. 10 Projection of coordinate-straining plane onto solution plane.

Because G depends on the (small) parameters δ and ν, Eq. (33) can be expanded in a secondary asymptotic sequence of equations relating to powers of δ and ν. The lowest-order (zero order in ε, δ, and ν) equation is (because $G_{\bar\zeta}$ is higher order)

$$\frac{\partial F_0^0}{\partial \bar\zeta} = 0 \tag{34}$$

which indicates that F_0^0 is analytic in the ζ plane. Conformal mapping can, therefore, be used to solve this lowest-order mixed boundary-value problem.

The mapping

$$w = (\zeta - b)/(\zeta - d), \qquad w \equiv u + iv$$

$$d \equiv \tfrac{1}{2}\left[1 - \delta^2 + \nu^2 + \sqrt{(1-\delta^2)^2 - 2\nu^2(1+\delta^2) + \nu^4}\right]$$

$$b \equiv \nu^2/d \tag{35}$$

transforms the straining plane of Fig. 6 to a semi-annular region in the lower-half w plane, as shown in Fig. 10. The radii of the semicircular arcs C_1 and C_2 are, respectively,

$$r = \nu/d, \qquad R = (1/\delta)(1 - \nu^2/d) = (1/\delta)(1 - \nu r) \tag{36}$$

In this domain the Dirichlet–Neumann boundary conditions are separated, namely,

$$\text{on} \quad C_1 : T = \text{const}, \qquad \text{on} \quad C_2 : T = \text{const}$$

$$\text{on} \quad \overline{AD} : \theta = 0, \qquad \text{on} \quad \overline{BC} : \theta = \alpha \tag{37}$$

There is the additional general condition that mass flux is bounded. For isentropic conditions, the peak mass flux which occurs at $M = 1$ is (for $\gamma = 1.4$)

$$(\rho q)_{\max} = [2/(\gamma+1)]^{\frac{1}{2}(\gamma+1)/(\gamma-1)} = 0.578704\ldots \tag{38}$$

The analytic solution satisfying the boundary conditions (37) is

$$F_0^0(\zeta) = (\alpha/\pi)\log(w) = (\alpha/\pi)\log[(\zeta - b)/(\zeta - d)] \tag{39}$$

This solution can be converted to a function of τ and $\bar\tau$ by means of the straining relation (31). This supports the earlier conjecture that there is a local dependence on $\bar\tau$ of the zero-order (in ε) solution that is lost in the straightforward asymptotic expansion process.

The real part of solution (39) is

$$T_0^0 = (\alpha/2\pi)\,\ell n\{[(\zeta - b)(\bar\zeta - b)]/[(\zeta - d)(\bar\zeta - d)]\} \tag{40}$$

At the compression corner ($\alpha \geq 0$),

$$T_0^0 = (\alpha/\pi)\,\ell n\, r = (\alpha/\pi)[\ell n\,\nu + \delta^2 + \cdots] \tag{41}$$

At the expansion corner,

$$T_0^0 = (\alpha/\pi)\,\ell n\, R = -(\alpha/\pi)[\ell n\,\delta + \nu^2 + \cdots] \tag{42}$$

Velocity is finite at the singular points and dependent on the parameters δ and ν. At $\tau = 0$, the value of T_0^0 for ramp angle α must be the same as that at $\tau = 1$ for ramp angle $-\alpha$. For stagnation to occur at the compression corner when $\alpha = \pi/2$, Eq. (41) implies r (and ν) must vanish. The parameters δ and ν can be used to enforce the mass flux condition (38). Intuitively, they should be small quantities, as suggested by the mapping (31) and the corner results (41) and (42).

Higher-order (nonsingular) solutions relating to the expansion parameters δ and ν can be generated readily. As expected, these solutions depend on both ζ and $\bar\zeta$ (and hence, τ and $\bar\tau$). As the singular points are approached, these solutions yield finite zero-order contributions, whose cumulative effect is logarithmically divergent. This breakdown is traceable to the fact that straightforward expansion of the straining function (31) is not valid as τ (or $\bar\tau$) approaches either of the singular points. This approach was taken in Ref. 4 in an attempt to achieve uniform validity. Although this secondary expansion approach offers some improvement over the solution (29), it is still not acceptable.

An alternate strategy (believed to be unique) consists of substituting the straining function (31) into the solution (39) and adding a function Φ chosen to make the combination agree asymptotically with the solution (29) to some desired order in δ and ν. As noted earlier, choosing a straining function is arbitrary to a certain extent. The zero-order solution then becomes

$$F_0 = \frac{\alpha}{\pi}\log\left[\frac{1}{2} - b + \frac{1}{2}(\tau-1)\sqrt{1 + \frac{2\delta^2(\tau+\bar\tau)}{(\tau-1)(\bar\tau-1)}}\right.$$

$$\left. + \frac{\tau}{2}\sqrt{1 + \frac{2\nu^2(2-\tau-\bar\tau)}{\tau\bar\tau}}\right]$$

$$- \frac{\alpha}{\pi}\log\left[\frac{1}{2} - d + \frac{1}{2}(\tau-1)\sqrt{1 + \frac{2\delta^2(\tau+\bar\tau)}{(\tau-1)(\bar\tau-1)}}\right.$$

$$\left. + \frac{\tau}{2}\sqrt{1 + \frac{2\nu^2(2-\tau-\bar\tau)}{\tau\bar\tau}}\right] + \frac{\alpha}{\pi}\Phi(\tau, \bar\tau; \delta; \nu) \tag{43}$$

Straightforward expansion for small δ and ν gives

$$F_0 = (\alpha/\pi)\{\log[\tau/(\tau-1)] + \phi_1 + \phi_2 + \cdots + \Phi\} \tag{44}$$

The first-order component ϕ_1 is

$$\phi_1(\tau, \bar\tau; \delta; \nu) = \left(\delta^2 \big/ D_0^2 D_1^2\right)\left[\tfrac{1}{2}\bar\tau(\tau - \bar\tau) - \tau\bar\tau^2\right]$$

$$-\left(\nu^2 \big/ D_0^2 D_1^2\right)\left[\tfrac{1}{2}(\bar\tau - 1)(2 - \tau - 3\bar\tau + 2\tau\bar\tau)\right] \tag{45}$$

where

$$D_0 \equiv \sqrt{\tau\bar\tau} = \sqrt{s^2 + n^2}$$

$$D_1 \equiv \sqrt{(\tau-1)(\bar\tau-1)} = \sqrt{(s-1)^2 + n^2} \tag{46}$$

The second-order component is

$$\phi_2(\tau, \bar\tau; \delta; \nu) = \left(\delta^4 \big/ D_0^4 D_1^4\right)\left[\tfrac{1}{8}\bar\tau^2(4\tau - 1)(\tau + \bar\tau)^2\right.$$

$$\left. + \tfrac{1}{2}\tau^2\bar\tau^2(\bar\tau - 1)(\tau + 2\bar\tau - 1)\right] + \left(\nu^4 \big/ D_0^4 D_1^4\right)$$

$$\times\left[\tfrac{1}{8}(4\tau - 3)(\bar\tau - 1)^2(2 - \tau - \bar\tau)^2\right.$$

$$\left. + \tfrac{1}{2}\bar\tau(\tau - 1)^2(\bar\tau - 1)^2(2 - \tau - 2\bar\tau)\right]$$

$$+ \left(\delta^2\nu^2 \big/ D_0^4 D_1^4\right)\bar\tau(\bar\tau - 1)\left[\tfrac{1}{2}\tau^2(\bar\tau - 1)(2 - \tau - \bar\tau)\right.$$

$$\left. + \tfrac{1}{4}(2\tau - 1)(\tau + \bar\tau)(2 - \tau - \bar\tau)\right.$$

$$\left. + \tfrac{1}{2}\bar\tau(\tau - 1)^2(\tau + \bar\tau) - (2\tau - 1)\tau\bar\tau(\tau - 1)(\bar\tau - 1)\right] \tag{47}$$

Higher-order components can be generated readily.

One possible form for the additive function Φ (to order δ^6, ν^6) is

$$\Phi = \phi_1(\phi_2/\phi_1 - 1)^{-1} \tag{48}$$

This function remains finite throughout the τ plane, including the singular points. Then Eq. (44) becomes (away from the singular points)

$$F_0 = (\alpha/\pi)\log[\tau/(\tau-1)] + \mathcal{O}(\delta^6, \nu^6) \tag{49}$$

Extension to higher order is straightforward. The purpose of the additive function Φ is to preserve the analytic character of the zero-order solution in an asymptotic sense, as the ζ-plane solution described earlier attempts to do. The imaginary part of Φ vanishes on the real axis, $n = 0$, so that the θ boundary conditions are unaffected.

At the singular points, Eq. (43) gives the results

$$\lim_{\tau\to 0}\{F_0\} = \frac{\alpha}{\pi}\ell_n r - \frac{2}{3}\frac{\alpha}{\pi} - \frac{i\alpha}{\pi}\left[\tan^{-1}\left(\frac{\nu\sin\psi}{\nu\cos\psi - d}\right) - \tan^{-1}\left(\frac{d\sin\psi}{d\cos\psi - \nu}\right)\right] \tag{50}$$

$$\lim_{\tau\to 1}\{F_0\} = \frac{\alpha}{\pi}\ell_n R + \frac{2}{3}\frac{\alpha}{\pi} + \frac{i\alpha}{\pi}\left[\tan^{-1}\left(\frac{\delta\sin\omega}{1-b+\delta\cos\omega}\right) - \tan^{-1}\left(\frac{\delta\sin\omega}{1-d+\delta\cos\omega}\right)\right] \tag{51}$$

Use has been made of the relations

$$\lim_{\tau\to 0}\left\{\frac{\tau}{\bar\tau}\right\} = e^{2i\psi}, \qquad \lim_{\tau\to 1}\left\{\frac{\tau-1}{\bar\tau-1}\right\} = e^{2i\omega} \tag{52}$$

The imaginary parts of the relations (50) and (51) have the correct discontinuity in surface θ boundary conditions across the singular points. Expressing these specific point solutions in terms of mass flux, at the expansion corner, $\tau = 1$,

$$(\rho q)_E = \rho_\infty q_\infty\left(e^{\frac{2}{3}}R\right)^{\alpha/\pi} \tag{53}$$

whereas at the compression corner, $\tau = 0$,

$$(\rho q)_C = \rho_\infty q_\infty\left(e^{-\frac{2}{3}}r\right)^{\alpha/\pi} \tag{54}$$

It remains to determine the parameters R and r (or the equivalent, δ and ν). The effect of compressibility on R and r can be expressed as

$$R^{|\alpha|/\pi} = R_0^{|\alpha|/\pi}\left[1 + \varepsilon R_1 + \varepsilon^2 R_2 + \cdots\right] \tag{55}$$

$$r^{|\alpha|/\pi} = r_0^{|\alpha|/\pi}\left[1 + \varepsilon r_1 + \varepsilon^2 r_2 + \cdots\right] \tag{56}$$

Absolute value of the exponents prevents inversion of these relations when α changes sign.

First-Order Solution

Solution of the first-order equation can be found by inspection and is given by Eq. (28). To first order, the solution for T is

$$T = T_0 + \varepsilon\left[1 - e^{2T_0}\right] \tag{57}$$

where T_0 is the real part of solution (43). At the expansion corner ($\tau = 1$; $\alpha > 0$), this solution in terms of mass flux becomes

$$(\rho q)_E = \rho_\infty q_\infty\left(e^{\frac{2}{3}}R_0\right)^{\alpha/\pi}\left\{1 + \varepsilon\left[1 + R_1 - \left(e^{\frac{2}{3}}R_0\right)^{2\alpha/\pi}\right]\right\} \tag{58}$$

Expansion (55) has been used in arriving at this result. For subsonic freestream Mach numbers, ε is small enough to justify series expansion of the exponential term involved.

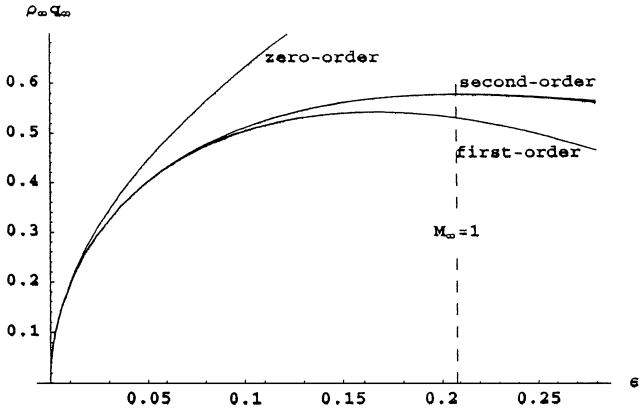

Fig. 11 Convergence characteristics of freestream mass flux expansion.

Freestream mass flux can be expressed in terms of the expansion parameter ε as

$$\rho_\infty q_\infty = 2\sqrt{\varepsilon}[1 - 2(\gamma-1)\varepsilon]^{1/(\gamma-1)} = 2\sqrt{\varepsilon}[1 - 2\varepsilon + 2(2-\gamma)\varepsilon^2 + \cdots] \tag{59}$$

This expansion converges rapidly, as shown in Fig. 11; the second-order approximation barely differs from the exact up to $M_\infty = 1$. This offers a strategy for enforcing the maximum mass flux condition (38) at the expansion corner. Introduction of expansion (59) into expansion-corner relation (58) gives

$$(\rho q)_E = 2\sqrt{\hat\varepsilon}\left\{1 - \hat\varepsilon\left[(1-R_1)\left(e^{\frac{2}{3}}R_0\right)^{-2\alpha/\pi} + 1\right]\right\} \tag{60}$$

where the similarity-type variable $\hat\varepsilon$ is defined as

$$\hat\varepsilon \equiv \varepsilon\left(e^{\frac{2}{3}}R_0\right)^{2\alpha/\pi} \tag{61}$$

Equation (60) emulates mass flux expansion (59) to first order if

$$R_1 = 1 - \left(e^{\frac{2}{3}}R_0\right)^{2\alpha/\pi} \tag{62}$$

which determines R_1 as a function of R_0 and α. Equation (58) then becomes

$$(\rho q)_E = \rho_\infty q_\infty\left(e^{\frac{2}{3}}R_0\right)^{\alpha/\pi}\left\{1 + 2\varepsilon\left[1 - \left(e^{\frac{2}{3}}R_0\right)^{2\alpha/\pi}\right]\right\} \tag{63}$$

Extension to higher order is straightforward.

At critical freestream Mach number M_∞^*, the expansion corner Mach number is 1, and Eq. (61) yields

$$\varepsilon^* = [1/2(\gamma+1)]\left(e^{\frac{2}{3}}R_0\right)^{-2\alpha/\pi} = \tfrac{1}{4}\left(M_\infty^*\right)^2\{1 + [(\gamma-1)/2]\left(M_\infty^*\right)^2\}^{-1} \tag{64}$$

This relation determines M_∞^* as a function of R_0 and α.

Second-Order Solution

From generating equation (18), the second-order (in ε) equation is

$$\frac{\partial F_2}{\partial\bar\tau} = \frac{1}{2}\frac{\partial}{\partial\tau}(U+V)_2 - \frac{1}{2}\frac{\partial}{\partial\bar\tau}(U-V)_2 \tag{65}$$

When expansions (12), (14) and (15) are introduced, the second-order solution component is

$$F_2 = \frac{2\gamma+1}{2}\left[1 - e^{4T_0}\right] - 2\left[1 - e^{2T_0}\right] + \frac{\gamma+1}{2}\frac{\partial}{\partial\tau}\int e^{4T_0}\,\mathrm{d}\bar\tau + H_2(\tau) \tag{66}$$

The first-order solution component (28) has been incorporated into this result. The analytic function $H_2(\tau)$ provides for maintaining boundary condition fidelity.

The contribution of the second-order component is very small and confined to the vicinity of the expansion corner $\tau = 1$ (as will be

evident later in the computational results). The integrand in Eq. (66) can be expanded in Taylor series about $\tau = 1$ to give

$$e^{4T_0} \sim \left(e^{\frac{2}{3}} R_0\right)^{4\alpha/\pi} \left[1 - (2\alpha/\delta\pi)\sqrt{(\tau-1)(\bar{\tau}-1)}\right] + \mathcal{O}[(\tau-1)^2] \tag{67}$$

Application of the integration–differentiation operations indicated in Eq. (66) yields

$$\frac{\partial}{\partial\tau}\int e^{4T_0}\,\mathrm{d}\bar{\tau} \sim -\frac{2\alpha}{3\delta\pi}\left(e^{\frac{2}{3}} R_0\right)^{4\alpha/\pi} \frac{(\bar{\tau}-1)^{\frac{3}{2}}}{\sqrt{\tau-1}} \tag{68}$$

Therefore, this term has no contribution at $\tau = 1$ and only minimal contribution in the neighborhood of $\tau = 1$. If the integral term is neglected, the second-order solution component becomes

$$F_2 = [(2\gamma+1)/2][1 - e^{4T_0}] - 2[1 - e^{2T_0}] = T_2 \tag{69}$$

where the zero-order solution component T_0 is the real part of solution (43). With this simplification the analytic function $H_2(\tau)$ in expression (66) is not needed because F_2 is real.

At the expansion corner, $\tau = 1$, extension of the mass flux relation (63) to second order yields

$$\begin{aligned}(\rho q)_E = {} & \rho_\infty q_\infty \left(e^{\frac{2}{3}} R_0\right)^{\alpha/\pi} \left\{1 + 2\varepsilon\left[1 - \left(e^{\frac{2}{3}} R_0\right)^{2\alpha/\pi}\right]\right. \\ & + \left(\tfrac{3}{2}\right)\varepsilon^2\left[1 - \left(e^{\frac{2}{3}} R_0\right)^{2\alpha/\pi}\right]^2 + [(2\gamma-3)/2]\varepsilon^2 \\ & \left.\times\left[1 - \left(e^{\frac{2}{3}} R_0\right)^{4\alpha/\pi}\right] + \varepsilon^2 R_2\right\}\end{aligned} \tag{70}$$

Expansion (55) has been incorporated along with first-order result (62). After the introduction of expansion (59), the resulting expression emulates the mass flux expansion if

$$R_2 = (\gamma-1)\left[1 - \left(e^{\frac{2}{3}} R_0\right)^{4\alpha/\pi}\right] + \left[1 - \left(e^{\frac{2}{3}} R_0\right)^{2\alpha/\pi}\right] \tag{71}$$

Equation (70) then becomes

$$\begin{aligned}(\rho q)_E = {} & \rho_\infty q_\infty \left(e^{\frac{2}{3}} R_0\right)^{\alpha/\pi} \left\{1 + 2\varepsilon(1+2\varepsilon)\left[1 - \left(e^{\frac{2}{3}} R_0\right)^{2\alpha/\pi}\right]\right. \\ & \left. - 2(2-\gamma)\varepsilon^2\left[1 - \left(e^{\frac{2}{3}} R_0\right)^{4\alpha/\pi}\right]\right\}\end{aligned} \tag{72}$$

To second order, expansions (55) and (56) may be written

$$\begin{aligned}R^{|\alpha|/\pi} = {} & R_0^{|\alpha|/\pi}\left\{1 + \varepsilon(1+\varepsilon)\left[1 - \left(e^{\frac{2}{3}} R_0\right)^{2\alpha/\pi}\right]\right. \\ & \left. + (\gamma-1)\varepsilon^2\left[1 - \left(e^{\frac{2}{3}} R_0\right)^{4\alpha/\pi}\right]\right\}\end{aligned} \tag{73}$$

and because $r(\alpha) = 1/R(-\alpha)$,

$$\begin{aligned}r^{|\alpha|/\pi} = {} & r_0^{|\alpha|/\pi}\left\{1 - \varepsilon(1-\varepsilon)\left[1 - \left(e^{-\frac{2}{3}} r_0\right)^{2\alpha/\pi}\right]\right. \\ & \left. - \gamma\varepsilon^2\left[1 - \left(e^{-\frac{2}{3}} r_0\right)^{4\alpha/\pi}\right]\right\}\end{aligned} \tag{74}$$

Extension to third-order allows the factors $e^{\pm 2/3}$ in these (and all preceding) expressions to be eliminated. Thus far, this factor always appears in the combination $e^{2/3}R_0$ or $e^{-2/3}r_0$, and eliminating the exponential factor allows these terms to be replaced by R_0 and r_0, respectively.

Corner Model

At the corner points the velocity (or momentum) vector rotates at constant magnitude through an angle α due to an impulsive-type interaction. This is illustrated by the generic model in Fig. 12. The corner (of turning angle Δ) can be either compressive or expansive.

Based on dimensional considerations, a corner-point momentum relation can be postulated having the form

$$\rho_c q_c^2 = M_\infty^2[h_1(\Delta)(p_\infty - p_c) + h_2(\Delta)p_c] \tag{75}$$

where ρ_c, p_c, and q_c are density, pressure, and velocity magnitude at the corner point. The functions $h_1(\Delta)$ and $h_2(\Delta)$ are to be determined. This model ignores any interaction between the compression and expansion corners of the ramp, which is justified on the basis

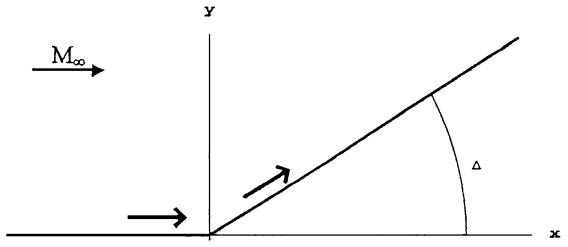

Fig. 12 Generic corner model.

that the geometric singularity effects are very local. (This will be evident later in the computational results.)

Equation (75) can be rewritten in terms of corner-velocity magnitude as

$$\begin{aligned}q_c^2\left\{1 - [(\gamma-1)/2]q_c^2\right\}^{1/(\gamma-1)} = {} & M_\infty^2(h_2 - h_1) \\ \times\left\{1 - [(\gamma-1)/2]q_c^2\right\}^{\gamma/(\gamma-1)} + {} & M_\infty^2 h_1\left\{1 - [(\gamma-1)/2]q_\infty^2\right\}^{\gamma/(\gamma-1)}\end{aligned} \tag{76}$$

Several properties of the functions h_1 and h_2 can be deduced from this expression, namely,

$$\begin{aligned}h_2 &= \left(e^{\frac{2}{3}} R_0\right)^{-2\Delta/\pi} && (\Delta \le 0, \tau = 1) \\ &= \left(e^{-\frac{2}{3}} r_0\right)^{2\Delta/\pi}, && (\Delta \ge 0, \tau = 0)\end{aligned} \tag{77}$$

$$h_2(0) = 1, \qquad h_1\left(\frac{\pi}{2}\right) = h_2\left(\frac{\pi}{2}\right) = 0$$

$$\left(\frac{\mathrm{d}h_1}{\mathrm{d}\Delta}\right)_{\Delta=\pi/2} = \left(\frac{\mathrm{d}h_2}{\mathrm{d}\Delta}\right)_{\Delta=\pi/2} = 0 \tag{78}$$

$$\left(\frac{\mathrm{d}r_0}{\mathrm{d}\Delta}\right)_{\Delta=\pi/2} = 0 \tag{79}$$

Note that $r_0 = 0$ when $\Delta = \pi/2$ (stagnation). Conditions (77) are obtained by equating the zero-order term of Eq. (76) with that of Eq. (72).

Application of model (76) to the ramp expansion corner ($\tau = 1$; $\alpha = -\Delta > 0$) at critical conditions gives

$$\begin{aligned}&[(\gamma+1)/2]^{\gamma/(\gamma-1)}[1 - 2(\gamma-1)\varepsilon^*]^{\gamma/(\gamma-1)} - 1 \\ &\quad = \left[1\Big/\left(4\varepsilon^* h_1\right)\right]\{[(\gamma-1)/(\gamma+1)] - 2(\gamma-1)\varepsilon^*\}\end{aligned} \tag{80}$$

Equations (64) and (77) have been used to eliminate h_2 in terms of ε^*. Application of L'Hospital's rule at $\alpha = 0$ gives the additional condition

$$h_1(0) = (\gamma-1)/\gamma \tag{81}$$

One possible form for h_1 that satisfies this condition along with those given in Eqs. (78) is

$$h_1(\alpha) = [(\gamma-1)/\gamma](1 + 2\alpha/\pi)^2(1 - \alpha/\pi)^{-2} \tag{82}$$

Note that $\alpha = -\Delta$ at the expansion corner. Equation (80) can then be solved for ε^* and R_0 obtained from Eq. (64). This assumed form for h_1 is justified because the corner model (76) is only an approximation of the very local effects of the geometric singularity. Accuracy of these assumptions can be verified by comparison with test data and corroboration with the von Kármán similarity rule.

Application of L'Hospital's rule to the α derivative of Eq. (80) provides the result

$$(R_0)_{\alpha=0} = e^{10/3} \tag{83}$$

With the assumption that compressibility has no effect on R_0 or r_0, the assumed relation

$$r_0 = e^{-10/3}(1 - 2\alpha/\pi)^2(1 - \alpha/\pi)^2 \tag{84}$$

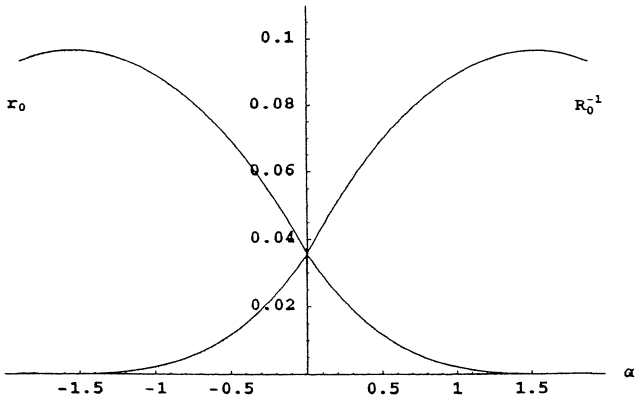

Fig. 13 Variation of R_0^{-1} and r_0 with ramp angle α.

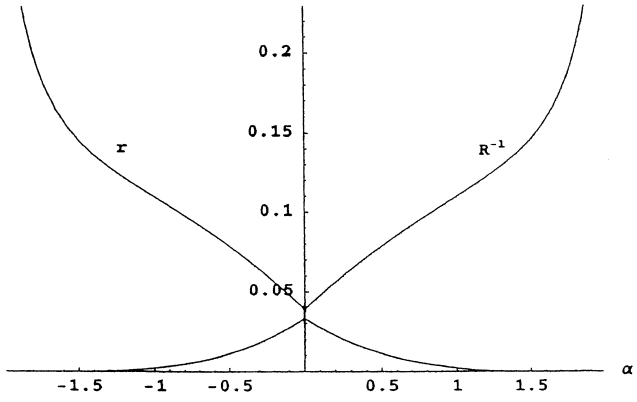

Fig. 14 Second-order variation of R^{-1} and r with ramp angle.

provides continuity between r_0 and R_0^{-1} across $\alpha = 0$. This form also satisfies condition (79) and vanishes at $\alpha = \pi/2$ (stagnation).

Variation with ramp angle of the parameters R_0^{-1} and r_0 obtained from Eqs. (64), (80), and (84) is shown in Fig. 13. These parameters are associated with $\tau = 1$ and $\tau = 0$, respectively. The magnitudes of the higher-order terms appearing in Eqs. (73) and (74) are not relatively large. The correction εR_1 is a maximum at critical Mach number, with its magnitude always less than 0.20; the magnitude of the correction $\varepsilon^2 R_2$ is always approximately less than 0.02. The variation to second order of R^{-1} and r with ramp angle is shown in Fig. 14 for $M_\infty = 0.20$, which is near critical Mach number for a forward-facing step (shown later). Note that critical Mach number for a circular cylinder is approximately 0.40. These quantities in Fig. 14 are discontinuous at $\alpha = 0$, which is indicative of a difference between the expansion and compression processes.

Normalized velocity is provided by expansions (14), whose components are given in Eqs. (15). To second order, the normalized velocity at the expansion corner ($\tau = 1$) is

$$(\bar{q})_E = \left(e^{\frac{2}{3}}R\right)^{\alpha/\pi}\left\{1 - \varepsilon(1-3\varepsilon)\left[1 - \left(e^{\frac{2}{3}}R\right)^{2\alpha/\pi}\right] - (\gamma+2)\varepsilon^2\left[1 - \left(e^{\frac{2}{3}}R\right)^{4\alpha/\pi}\right]\right\} \tag{85}$$

Introduction of expansion (73), definition (11), and Eq. (64) reduces this result to

$$(\bar{q})_E = \left(e^{\frac{2}{3}}R_0\right)^{\alpha/\pi} + \mathcal{O}(\varepsilon^3)$$

$$(q)_E = \sqrt{[2/(\gamma+1)](\varepsilon/\varepsilon^*)} + \mathcal{O}(\varepsilon^3) \tag{86}$$

At critical freestream Mach number, this becomes

$$(q)_E = \sqrt{2/(\gamma+1)} \tag{87}$$

which corresponds to a local Mach number of 1.

Results and Discussion

The present analysis removes the singular, nonphysical behavior from the classical ramp flow solution (29) at both the compression and expansion corners. Computational results that illustrate the consistency of the analysis along with its convergence characteristics are presented in this section. Corroboration with the von Kármán similarity rule and comparison with experimental results are also presented.

Computational Results

Figure 15 shows the surface, $n = 0$, distribution of T to zero, first, and second order for a ramp angle of $\pi/4$ (45 deg) and a freestream Mach number of 0.30. Convergence is rapid and the higher-order effects are very local. Normalized surface velocity $\bar{q}$ for these same conditions is shown in Fig. 16. The classical singular distribution from solution (29) is also shown for comparison. The zero-order solution is independent of M_∞ and the first- and second-order corrections are extremely small. Note the nearly order independence of the velocity at the expansion corner, as indicated by result (86). Further validation of this result is presented in Fig. 17, which shows the variation with ramp angle of local Mach number at the expansion corner at critical freestream Mach number. The second-order error is at most about 1%. For completeness, the variation with ramp angle of the compression corner Mach number at critical freestream conditions is presented in Fig. 18. Zero-, first-, and second-order results are shown.

Corroboration with Von Kármán Similarity Rule

The present analysis can be confirmed within the frame-work of the von Kármán similarity rule. This rule (as stated in Ref. 5) is derived from a first-order potential flow analysis under the assumption of small perturbations from freestream conditions. It has been validated extensively by experiment. The rule states that if body thickness ratio t (assumed small) and freestream Mach number are

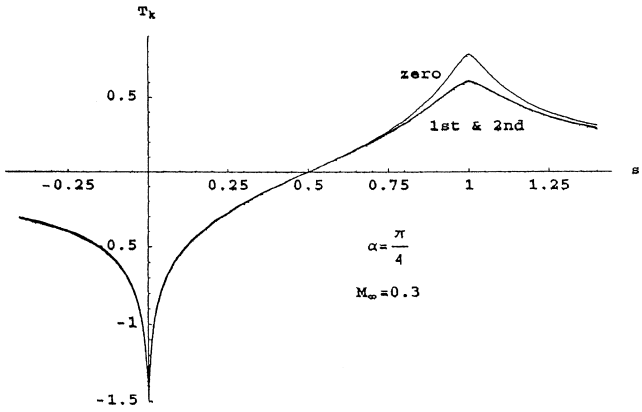

Fig. 15 Zero-, first- and second-order surface variation of T.

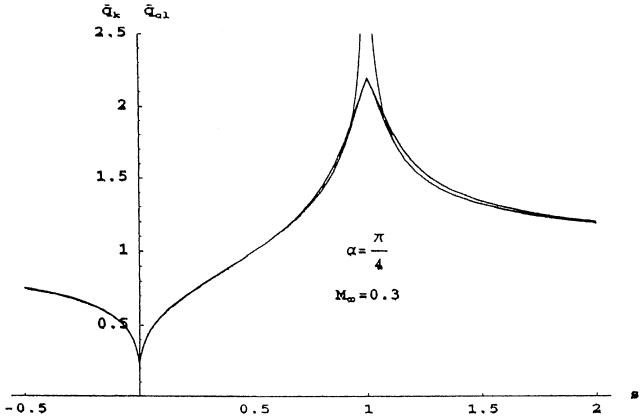

Fig. 16 Variation of normalized surface velocity.

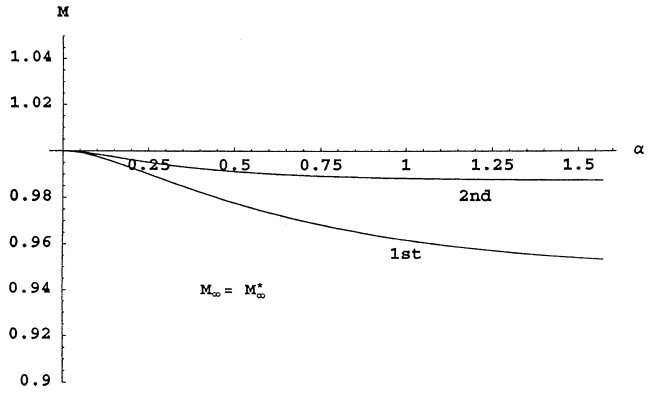

Fig. 17 Expansion corner Mach number variation with ramp angle at critical conditions.

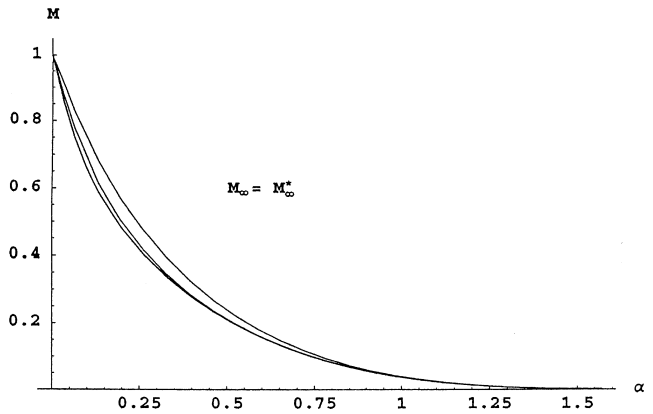

Fig. 18 Compression corner Mach number variation with ramp angle at critical conditions.

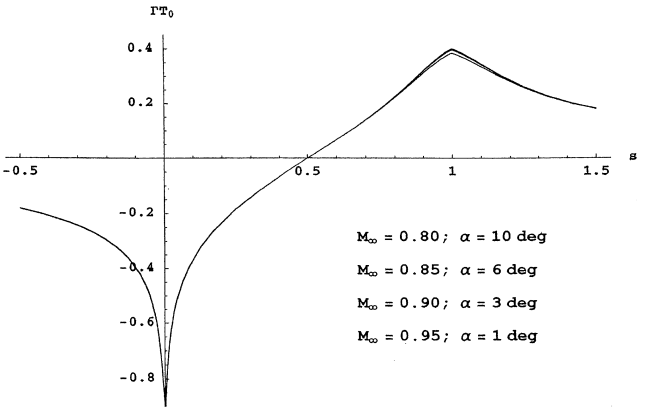

Fig. 19 Corroboration with von Kármán similarity rule.

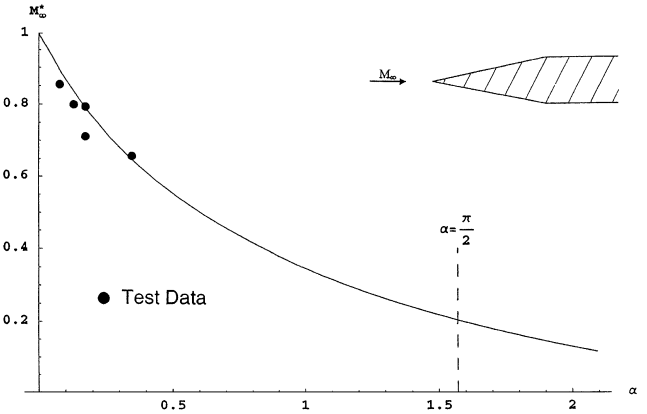

Fig. 20 Critical Mach number variation with ramp angle and comparison with experimental data.

adjusted so that the similarity parameter

$$\lambda \equiv \frac{tM_\infty^2}{\left(\left|1-M_\infty^2\right|\right)^{\frac{3}{2}}} \tag{88}$$

remains constant, then solutions for members of a given family of bodies are the same, that is, depend in the same way on the spatial coordinates, when scaled by the parameter

$$\Gamma(M_\infty) \equiv M_\infty^2 \Big/ \left(\left|1-M_\infty^2\right|\right)^{\frac{3}{2}} \tag{89}$$

Freestream Mach number is unrestricted. For the ramp flow problem (small) thickness ratio is $\tan\alpha \approx \alpha$.

With reference to Eqs. (12), to first order

$$U = -V = \varepsilon\bar{q}^2 \tag{90}$$

so that Euler system (9) to first order may be written in the Cauchy–Riemann form:

$$\frac{\partial\theta}{\partial s} - \frac{\partial}{\partial n}[T-\varepsilon(1-\bar{q}^2)] = 0, \qquad \frac{\partial\theta}{\partial n} + \frac{\partial}{\partial s}[T-\varepsilon(1-\bar{q}^2)] = 0 \tag{91}$$

Therefore, to first order [see Eq. (57)]

$$T-\varepsilon(1-\bar{q}^2) = T_0(s,n,\alpha,R,r) + \mathcal{O}(\varepsilon^2) \tag{92}$$

where T_0 is the real part of solution (43) and first-order approximations are to be used for R and r. Application of the similarity-rule arguments to Eq. (91) results in

$$\Gamma(M_\infty)[T_0 - i\theta_0] = \text{function}(s,n;\lambda) \tag{93}$$

Note that the first-order correction to θ is zero.

The variation of ΓT_0 (with λ held constant) along the solid boundary is shown in Fig. 19 for four values of M_∞, namely, 0.80, 0.85, 0.90, and 0.95. The corresponding ramp angles obtained from Eq. (88) are approximately 10, 6, 3, and 1 deg, respectively. The scaled solutions are nearly identical; for angles larger than 10 deg, noticeable deviations first appear at the expansion corner. Local Mach number at the expansion corner varies from 0.97 to 1.01 for these four solutions. For the 10-deg ramp solution (which shows a slight deviation), this represents approximately a 25% perturbation from freestream conditions. These results serve to validate the assumptions made in deriving the local corner model.

Comparison with Experiment

Experimental data for compressible flow past wedges with straight afterbodies are presented in Refs. 8 and 9. For a wedge geometry, viscous effects will prevent an accurate assessment at the leading edge (compression corner), but will be meaningful at the expansion corner. Figure 20 compares predicted critical Mach number (at the expansion corner) obtained from Eq. (80) with data extracted from these references. The comparison is favorable, although the range of experimental wedge (ramp) angles is limited.

To compare with experimental surface distributions, the theoretical solution must be mapped to the physical plane solid boundary by the relation

$$\sigma = \int \frac{1}{q}\,\mathrm{d}s \tag{94}$$

where σ is arc length along the surface. This integration is best carried out numerically.

Surface Mach number predictions are compared in Fig. 21 with measurements taken from Ref. 8 for a 10-deg half-angle wedge with a straight afterbody. These (wedge) surface data were inferred from interferometer measurements of density and actually correspond

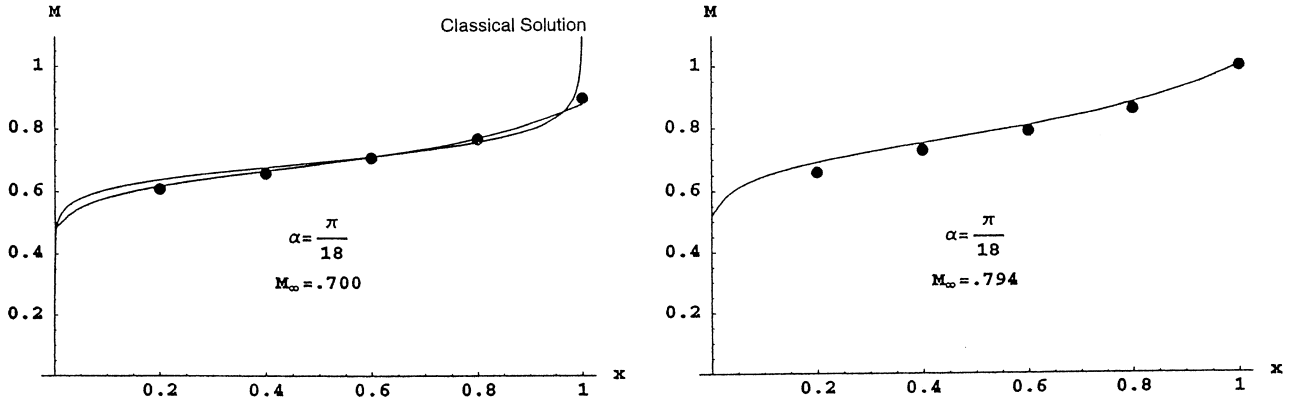

Fig. 21 Comparison of surface Mach number predictions with experimental data.

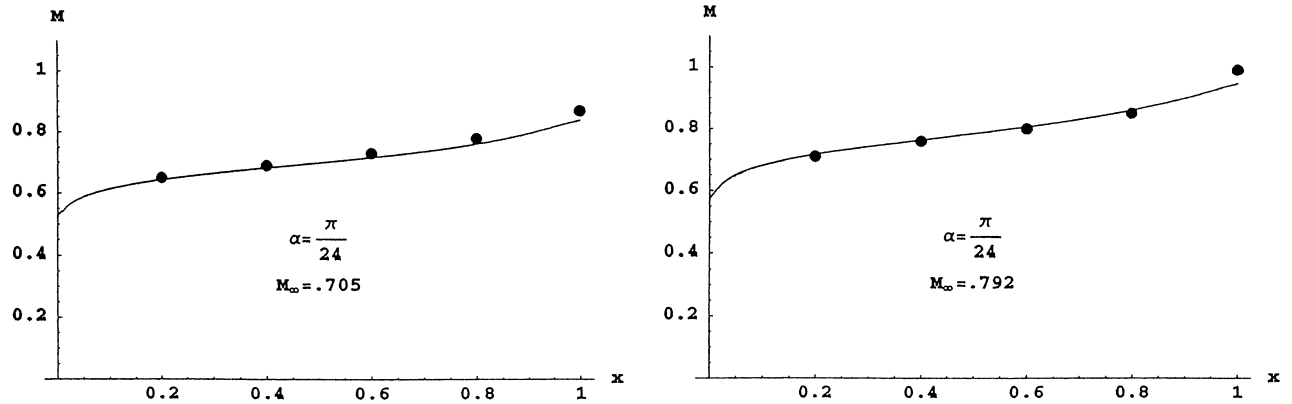

Fig. 22 Comparison of surface Mach number predictions with experimental data.

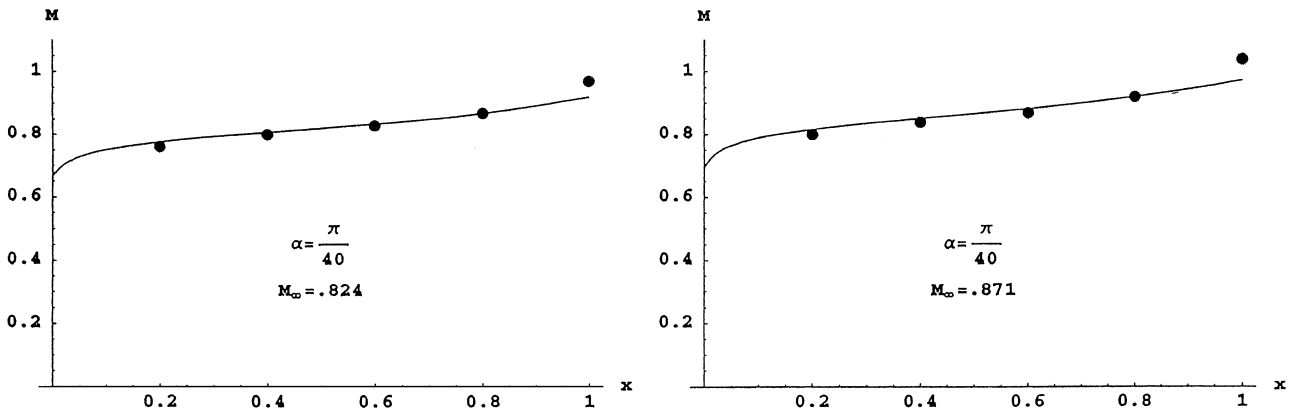

Fig. 23 Comparison of surface Mach number predictions with experimental data.

to (approximately) the edge of the boundary layer displacement thickness. The boundary layer was laminar and was relatively thin because of the favorable pressure gradient induced by the inclined wedge surface. Agreement is favorable except toward the leading edge, where the boundary layer produces a slight rounding effect. The freestream Mach number was very close to critical for the higher-Mach-number case. The classical result derived from solution (29) is shown for comparison for the lower-Mach-number case.

Comparisons for a $7\frac{1}{2}$-deg half-angle wedge are shown in Fig. 22. Results for a $4\frac{1}{2}$-deg half-angle wedge are compared in Fig. 23; the higher Mach number case was slightly supercritical. The pressure gradient is less favorable for these thinner geometries, so that the boundary layer is relatively thicker.

These comparisons provide some validation for the assumptions made in developing the local corner model. Verification at the compression corner will be difficult because of viscous effects; however, the predictions have more merit than the nonphysical results of the classical solution (29).

Conclusions

A newly developed procedure for deriving analytical, asymptotic solutions of the two-dimensional steady Euler equations has been applied to compressible, subsonic flow past a ramp of arbitrary inclination angle. The Euler formulation has mass flux and flow angle as dependent variables, which offers distinct advantages over more conventional variable choices. Higher-order singularity compounding at the expansion and compression corners of the ramp inherent in the classical solution is analytically removed by means of a non-conformal complex-variable coordinate straining, and a new strategy is introduced to ensure uniform validity. This analysis can provide the basis for improving inviscid CFD surface boundary conditions near corners, for example, airfoil trailing edge.

Second-order solutions are derived that circumvent the inconsistencies arising from applying incompressible models to describe flow behavior near geometric singularities. Mass flux at the expansion corner remains bounded as a consequence of the new Euler formulation. Computational results are presented that illustrate the consistency and convergence characteristics of the present analysis. The analysis is also well corroborated into the transonic shock-free range by the von Kármán similarity rule. Predictions of surface Mach number for compressible flow past slender wedges with straight afterbodies compare favorably with experimental measurements, even for slightly supercritical conditions. Critical Mach number predictions also compare well with test data for these type bodies.

References

[1]Verhoff, A., Cary, A., and Epstein, R., "A New Approach for Efficient Construction of Asymptotic Solutions of the Two-Dimensional Euler Equations," AIAA Paper 98-0122, Jan. 1998.

[2]Verhoff, A., and Cary, A., "An Analytical Asymptotic Solution Method for 2D Transonic Inviscid Flow," AIAA Paper 99-0173, Jan. 1999.

[3]Verhoff, A., Stookesberry, D., and Michal, T., "Hodograph Solutions for Compressible Flow past a Corner and Comparison with Euler Numerical Predictions," AIAA Paper 91-1547, June 1991.

[4]Verhoff, A., and Cary, A., "Analytical Euler Solutions for 2D Flows with Corners Using Asymptotic Methods," AIAA Paper 98-2687, June 1998.

[5]Liepmann, H. W., and Roshko, A., *Elements of Gasdynamics*, Wiley, New York, 1957, Chap. 10.

[6]Lighthill , M. J., *Higher Approximations in Aerodynamic Theory*, Princeton Univ. Press, Princeton, NJ, 1960, Sec. E.

[7]Van Dyke, M., *Perturbation Methods in Fluid Mechanics*, Academic Press, New York, 1964, Chap. 6.

[8]Bryson, A. E., "An Experimental Investigation of Transonic Flow past Two-Dimensional Wedge and Circular Arc Sections Using a Mach–Zehnder Interferometer," NACA TN 2560, Nov. 1951.

[9]Pack, D. C., and Groth, E., "Investigation of the Flow past Finite Wedges of 20 deg and 40 deg Apex Angle at Subsonic and Supersonic Speeds, Using a Mach-Zehnder Interferometer," British Aeronautical Research Council, ARC R&M 2321, May 1946.

M. Sichel
Associate Editor